IEEE Access
Multidisciplinary | Rapid Review | Open Access Journal

Received December 13, 2020, accepted December 29, 2020, date of publication January 5, 2021, date of current version January 15, 2021.

Digital Object Identifier 10.1109/ACCESS.2021.3049448

Defect Recognition in Concrete Ultrasonic Detection Based on Wavelet Packet Transform and Stochastic Configuration Networks

JINHUI ZHAO[1,2], (Member, IEEE), TIANYU HU[2], RUIFANG ZHENG[2], PENGHUI BA[2], CONGLI MEI[1], AND QICHUN ZHANG[3], (Senior Member, IEEE)

[1]College of Electrical Engineering, Zhejiang University of Water Resources and Electric Power, Hangzhou 310018, China
[2]College of Mechanical and Electrical Engineering, China Jiliang University, Hangzhou 310018, China
[3]Department of Computer Science, University of Bradford, Bradford BD7 1DP, U.K.

Corresponding author: Jinhui Zhao (jhzhao2009@zju.edu.cn)

This work was supported in part by the Zhejiang Provincial Natural Science Foundation (ZJNSF) project under Grant (No. LY18F030012), the National Natural Science Foundation of China projects (NSFC) under Grant (No. 61403356, 61573311).

ABSTRACT Aiming to detect concrete defects, we propose a new identification method based on stochastic configuration networks. The presented model has been trained by time-domain and frequency-domain features which are extracted from filtering and decomposing ultrasonic detection signals. This method was applied to ultrasonic detection data collected from 5 mm, 7 mm, and 9 mm penetrating holes in C30 class concrete. In particular, wavelet packet transform (WPT) was then used to decompose the detected signals, thus the information in different frequency bands can be obtained. Based on the data from the fundamental frequency nodes of the detection signals, we calculated the means, standard deviations, kurtosis coefficients, skewness coefficients, and energy ratios to characterize the detection signals. We also analyzed their typical statistical features to assess the complexity of identifying these signals. Finally, we used the stochastic configuration networks (SCNs) algorithm to embed four-fold cross-validation for constructing the recognition model. Based upon the experimental results, the performance of the presented model has been validated and compared with the genetic algorithm based on BP neural network model, where the comparison shows that the SCNs algorithm has superior generalization abilities, better fitting abilities, and higher recognition accuracy for recognizing defect signals. In addition, the test and analysis results show that the proposed method is feasible and effective in detecting concrete hole defects.

INDEX TERMS Concrete defects, ultrasonic detection, wavelet packet transform, stochastic configuration networks, pattern recognition.

I. INTRODUCTION

Concrete is essential material in modern architecture. Indeed, it is widely used in the construction of many facilities, including buildings, bridges, and dams. After a certain period of use or degradations caused by natural disasters, the structure of concrete will deteriorate, thereby resulting in common problems such as internal voids and cracks. While there are several common non-destructive testing methods for these issues, such as ultrasound, ground-penetrating radar, and impact-echo [1], However, the ultrasonic method is not susceptible to environmental interference and is also considered a mature technology for inspecting issues such as weld quality [2]. After the ultrasonic propagates in the concrete, the waveform of the signal is diverse and the components in the signal are complex subjected to high-frequency noise. This will make it difficult for us to extract effective information from the signal, and it is also difficult to classify the detected signal. The existing manual recognition methods are low efficient and the traditional intelligent recognition methods have low accuracy. Therefore, it is a difficult and important task to extract the effective features of the complex signal so that we can identify the type of concrete ultrasonic detection signal faster with high accuracy.

Although some scholars have successfully modeled ultrasonic probes and obtained analog detection signals [3], there is currently no mechanism model for ultrasonic propagation in concrete. Due to the complexities of concrete components and structures, it is difficult to establish a precise model. At present, it is not feasible to analyze the actual

The associate editor coordinating the review of this manuscript and approving it for publication was Lefei Zhang.

concrete ultrasonic detection signal through the mechanism model. Nevertheless, a common method of data processing involves the extraction of effective information from detection data. In the study of hyperspectral images, the methods of extracting discriminative feature information based on local geometric structure Fisher analysis (LGSFA) [4] and local neighborhood structure preserving embedding (LNSPE) [5] effectively reduce the data dimension and improve the classification performance of the model. Mostavi *et al.* used wavelet transform and machine learning to analyze and identify ultrasonic signals [6], thus establishing an effective method, and machine learning identifies the processed ultrasonic signals and achieves high recognition accuracy. Traditional machine learning algorithms such as neural network and support vector machine have been used in concrete ultrasonic detection signal recognition cases [7]–[9]. However, these algorithms are not of sufficient accuracy for identifying complex concrete defect signals. Signal processing before identifying the signal is helpful to improve the recognition ability of the model. Fourier transform is often used in signal processing, but it has insufficient processing power for complex non-stationary signals [10]. Empirical mode decomposition will result in mode mixing when processing signals [11]. Some other studies have applied Kalman filtering or particle filtering in the context of ultrasonic signal processing. However, these signal processing methods are mostly used in target tracking, fault diagnosis, inertial navigation systems and other fields.

Deep learning is now a widely used intelligent recognition method that is associated with high accuracy and stability. There have been many such applications in the field of ultrasonic testing [12], [13]. However, this method requires large amounts of training data and contains many hidden layers. In this regard, large-scale datasets result in time-consuming training processes in the context of deep learning. It lacks of interpretability for different practical application models. Wang *et al.* proposed stochastic configuration networks with supervision mechanisms in 2017 [14], [15]. Such a network does not need to determine the optimal network structure parameters through an optimization algorithm and still has great generalization capabilities with samples containing noise and outliers. Wang *et al.* used handwritten digit recognition as an example to test SCNs, with results showing higher recognition accuracy and faster calculation speeds in addition to suitability for use in large-scale data-processing applications. Moreover, Qu *et al.* used stochastic configuration networks to diagnose the causes of fiber damage using optical fiber vibration signals [16]. It has been shown that the advantages of SCNs for pattern recognition.

To address the problem of low automation and low accuracy in the recognition of concrete ultrasonic detection signals, this study developed and assessed an ultrasonic processing and recognition method. The method is based on wavelet packet transform and the stochastic configuration networks. In particular, this method is used to conduct signal decomposition for the purpose of identifying typical concrete defects. At first, we used wavelet packet transform to decompose 360 ultrasonic signals obtained from a sample block of C30 class concrete. The coefficients of fundamental frequency node were selected to reconstruct the signal, while the mean value, standard deviation, kurtosis coefficient, skewness coefficient, and energy ratio were extracted to form a multi-dimensional joint feature vector. Then the vector was used as an input for training and testing the stochastic configuration networks model. A comparison was given with the BP neural network where the parameters have been optimized via genetic algorithm. The comparison results have been considered as a performance analysis for recognizing concrete defects. Experimental results showed that the method described in this article can effectively identify defective concrete ultrasonic detection signals. Compared with the traditional method BP neural network, the presented method has faster recognition speed and higher accuracy. In other words, using this method can greatly improve the detection efficiency and accuracy of concrete internal defects. As a result, it reflects the significance of practical engineering applications.

The remainder of this article is organized as follows. In section II, we describe all algorithmic steps and data-feature selections used in this study. In section III, we introduce the experimental environment and algorithmic parameter configurations. In section IV, we analyze the extracted features and discuss the defect recognition tests. Finally, section V presents our conclusions.

II. BASIC STEPS AND ALGORITHM FLOWCHART FOR THE PROPOSED ALGORITHM

In order to identify the concrete ultrasonic detection signal accurately, the presented algorithm consists of three parts. Firstly, we use wavelet packet transform to remove noises in the signals and retain useful information as much as possible. Then, effective features are extracted from the processed signals. Finally, the SCNs model is used to classify detection signals according to features. The main steps of the algorithm are described in the following subsections.

A. WAVELET PACKET TRANSFORM

The wavelet packet theory is based on the concept of orthogonal wavelet transform. Compared with wavelet transform, wavelet packet transform is a more refined method of signal analysis [17], [18]. Particularly, it decomposes the detection signal into two parts as low-frequency and high-frequency. The high-frequency part is then further decomposed, which is not performed in wavelet transform. Thus, this procedure overcomes issues of low time-frequency resolutions. Therefore, wavelet packet transform is more suitable than wavelet transformation for signal processing with higher practical potentials. We used wavelet packet transform to decompose the detection signal and selected the low-frequency node for reconstruction, which can filter out the high-frequency noise in the original signal and reduce the redundant information in the signal.

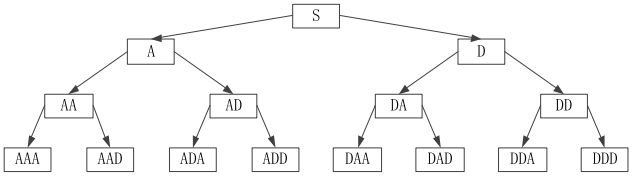

FIGURE 1. Three-layer wavelet packet decomposition diagram.

1) SIGNAL DECOMPOSITION OF WAVELET PACKET TRANSFORM

In Fig.1, S is the original signal, which is decomposed into A and D via wavelet packet decomposition. A is the low-frequency component resulting from the signal decomposition process, while D is the high-frequency component. According to the same method, the high-frequency and low-frequency components are continuously decomposed, then the original signal is ultimately decomposed into eight different frequency bands (i.e. after three-layer decompositions).

Wavelet packet decomposition projects the signal to the wavelet packet base to obtain the wavelet packet coefficient sequence. The cost function is then used to select the optimal wavelet packet basis. The smaller the value of the cost function, the better the implemented wavelet packet basis and the greater the effect on signal decomposition [19]. Currently, the most common cost function is Shannon entropy.

2) WAVELET BASIS FUNCTION SELECTION

To conduct wavelet packet decomposition on an ultrasonic detection signal, an appropriate wavelet basis function must be selected. In this regard, the Daubechies (dbN) wavelet function has better tight support, approximate symmetry, and smoothness [20], which can sufficiently represent the non-stationary state change process of ultrasonic defect signals in the time-frequency distribution. This study selected the db15 wavelet (named in MATLAB®) as the basis function of wavelet packet transform based on the characteristics of the actual detection signal data.

3) THE BASIC STEPS OF SIGNAL WAVELET PACKET TRANSFORM

The following content is a summary of the main steps involved in the decomposition and reconstruction algorithms, as provided in MATLAB® software:

1) Selecting the appropriate wavelet basis function and decompose the given signal to obtain the wavelet packet coefficient;

2) Selecting the optimal wavelet packet basis according to the cost function;

3) Repeating steps 1 and 2 to obtain a three-layer wavelet packet decomposition tree, as shown in Fig. 1;

4) Extracting the coefficient of the first node AAA of the third layer from the result of step 3;

5) According to the extracted wavelet packet coefficients, a reconstructed signal is obtained using a wavelet packet reconstruction algorithm.

B. ULTRASONIC SIGNAL FEATURES SELECTION

Data feature extraction is an important premise of machine learning. Feature extraction is to extract representative information in the signal. Through the feature information, the difference of various types of signals can be distinguished. Effective data features can facilitate the recognition model in accurately identifying defect signals. When ultrasonic waves propagate in defective concrete, their waveforms' dimensions in time-domain and frequency domain will be changed. For instance, Guo *et al.* extracted the shape factor, crest factor, impulse factor, and clearance factor of the signal as features for identifying aluminum plate crack defects [21], while Wang *et al.* extracted the average peak spacing, amplitude coefficient, dominant frequency, and attenuation coefficient for defect identification [22]. Note that these latter features are more suitable in the context of weld inspection.

Based on typical features [23], this study used the mean values, standard deviations, kurtosis coefficients, skewness coefficients, and energy ratios of each node after conducting wavelet packet transformation to characterize differences in the detection signal data. The calculation formula has been presented as follows:

Mean value is an indicator that reflects the trend of waveform signal data.

$$\bar{z} = \frac{1}{N}\sum_{i=1}^{N} z_i \tag{1}$$

where z_i and N denote the amplitude of the reconstructed signal and the number of sample points, respectively.

The standard deviation is the arithmetic square root of the variance and reflects the degree of dispersion of a waveform.

$$\sigma = \sqrt{\frac{1}{N}\sum_{i=1}^{N}(z_i - \bar{z})^2} \tag{2}$$

The kurtosis coefficient is used to characterize the peak height of the probability density distribution curve at the average.

$$ku = \frac{\sum_{i=1}^{N}(z_i - \bar{z})^4}{N\sigma^4} \tag{3}$$

The skewness coefficient is a statistical parameter that indicates the degree of data asymmetry.

$$sk = \frac{\sum_{i=1}^{N}(z_i - \bar{z})^3}{N\sigma^3} \tag{4}$$

The energy ratio represents the proportion of the signal in each frequency domain segment.

$$P = \frac{\sum_{i=1}^{N}|z_i|^2}{\sum_{k=0}^{2^j-1}\sum_{i=1}^{N}|z_i|^2} \tag{5}$$

where j stands for the number of wavelet packet decomposition layers.

In this study, the features extracted by wavelet packet transform were linearly normalized, while the original data were mapped between [0,1]. The normalized features were used as input variables for the neural network.

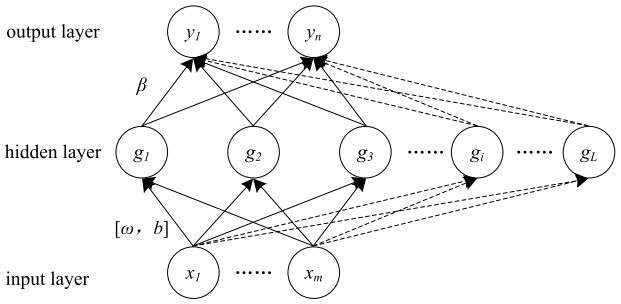

FIGURE 2. Stochastic configuration networks (SCNs) structure diagram.

C. STOCHASTIC CONFIGURATION NETWORKS

SCNs is a standard 3-layer forward feedback network structure consisting of an input layer, a hidden layer and an output layer. The standard model for SCNs is shown in Fig. 2, where $\boldsymbol{x}$ is the network input vector, $\boldsymbol{y}$ is the network output vector, ω and $\boldsymbol{b}$ are the weight and bias vectors of the input layer to the hidden layer, respectively, β is the weighting vector of the hidden layer to the output layer, g_i is the output of the i-th hidden node, and L is the number of hidden nodes. As mentioned earlier, we used the SC-III algorithm for SCNs [14], [15], [24].

In particular, the design flow has been recalled in this session [14]:

1) Given a target function $f: R^m \rightarrow R^n$, suppose that we have already built a single layer feed-forward network with L-1 hidden nodes:

$$f_{L-1}(x) = \sum_{i=1}^{L-1} \beta_i \cdot g_i(\omega_i^T x + b_i) \tag{6}$$

where $x = [x_1, \ldots, x_m]$, $\omega_i = [\omega_{i1}, \ldots, \omega_{im}]^T$, $\beta_i = [\beta_{i1}, \ldots, \beta_{in}]^T, f_0 = 0$, while $L = 2, 3, \ldots$.
Denoting residuals $e_{L-1} = f - f_{L-1} = [e_{L-1,1}, \ldots, e_{L-1,n}]^T$. If $f_L(X) = f_{L-1}(X) + \beta_L \cdot g_L(\omega_L^T \cdot X + b_L)$ fails to satisfy the given error criterion, then a new hidden node must be added into the existing hidden layer. In particular, a set of parameters $f_L(X) = f_{L-1}(X) + \beta_L \cdot g_L(\omega_L^T \cdot X + b_L)$ is added such that the approximation function is updated as follows:

$$F_L(x) = f_{L-1}(x) + \beta_L \cdot gL\left(\omega_L^T x + b_L\right) \tag{7}$$

2) To add a new hidden node, the input weight vector ω_L and bias b_L are randomly generated which satisfy the following inequality:

$$\sum_{q=1}^{n} \left\langle e_{L-1,q}, g_L^* \right\rangle^2 \geq \left\| g_L^* \right\|^2 \delta_L \tag{8}$$

where $g_L^* = g_L(\omega_L^T x + b_L)$, $\delta_L = (1 - r - \mu_L) \left\| e_{L-1} \right\|^2$, while $0 < r < 1$, $\lim_{L \rightarrow \infty} \mu_L = 0$ and $\mu_L = \frac{1-r}{L+1}$. Note that $\|\cdot\|$ denotes the L_2 norm, and $\langle \cdot \rangle$ stands for the inner product. In practice, the choice of r can be done as a real number as close to 1 as possible to meet the inequality condition (8).

If $\min\left\{\xi_{L,1}, \xi_{L,2}, \ldots, \xi_{L,n}\right\} \geq 0$, then we save ω_L and b_L as new weights and thresholds of the added hidden node, where

$$\xi_{L,q} = \frac{\left(e_{L-1,q}^T(x) \cdot h_L(x)\right)^2}{h_L^T(x) \cdot h_L(x)} - (1 - r - \mu_L)\, e_{L-1,q}^T(x) \cdot e_{L-1,q}(x) \tag{9}$$

where $h_L(x) = \left[g_L(\omega_L^T x_1 + b_L), \ldots, g_L(\omega_L^T x_N + b_L)\right]^T$.

3) Calculating the output weight:

$$\beta_{L,q} = \frac{\left\langle e_{L-1,q}, g_L \right\rangle}{\left\| g_L \right\|^2}, \quad q = 1, 2, \ldots, n \tag{10}$$

4) Updating the output weight β_L and using the standard least squares method to compute the output weights:

$$\begin{aligned} [\beta_1^*, \ldots, \beta_L^*] &= \arg\min_{\beta} \left\| f - \sum_{i=1}^{L} \beta_i \cdot g_i(\omega_i^T x + b_i) \right\|_F^2 \\ &= \arg\min_{\beta} \left\| H^T \beta - E \right\|_F^2 \\ &= H^{\dagger} E \end{aligned} \tag{11}$$

where $\beta_i^* = [\beta_{i,1}^*, \ldots, \beta_{i,n}^*]^T$, $H = [H_1, \ldots, H_L]^T$, while $H_i = [g_{i,1}, \ldots, g_{i,m}]^T$, $\|\cdot\|_F$ denotes the Frobenius norm, $\boldsymbol{E}$ is the $m \times n$ dimensional sample result matrix, and $H^{\dagger}$ stands for the Moore-Penrose generalized inverse.

5) Calculating the error in step L. If it is less than the pre-specified error criterion, the SCNs model training is completed; otherwise, continue to add hidden layer nodes according to step 2 until the error criterion is met or the set maximum number of hidden layer nodes is reached. When a new hidden node is generated, the parameters of other nodes have been determined which remain unchanged.

D. ALGORITHM FLOWCHART

To summarize the presented method, the flowchart is given as follow:

III. EXPERIMENTAL ENVIRONMENT AND TESTING

The detection data used in this study were obtained from the ultrasonic testing system via the transmission detection method. Basically, this system uses a P28F ultrasonic probe with a central frequency of 50 kHz; the ± 80V square wave pulse signal generated then excites the ultrasonic probe at the transmitting end.

The square wave pulse is given with short rise time and fall time. It can quickly excite the piezoelectric wafer [25]. The square wave pulse has good properties in terms of controllability and tuning [26]. The duty cycle of the square wave pulse is 0.25%. We set the signal sampling frequency to 1 MHz at the receiving end. The sample block used with the testing system was made from C30 class concrete, as shown in Fig. 4. The block was constructed using a customized architectural structure of mixed ordinary Portland cement type I, water,

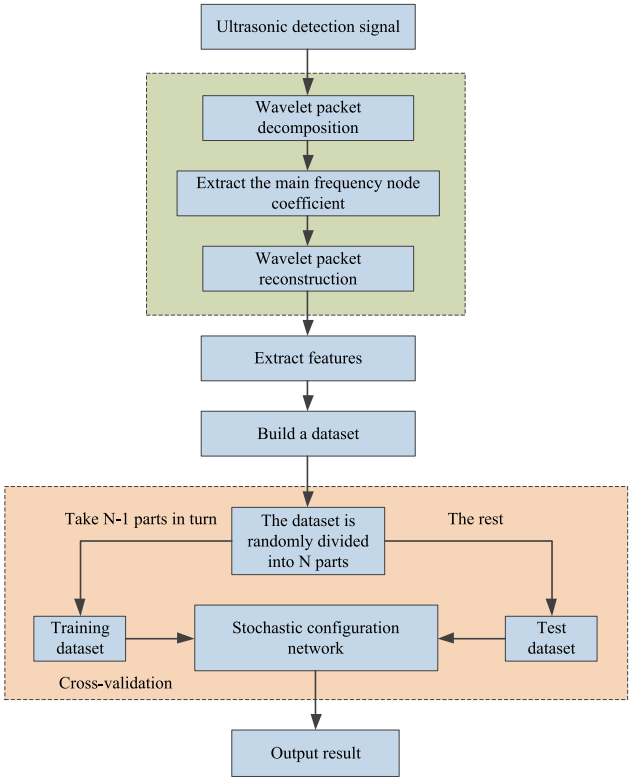

FIGURE 3. Algorithm flowchart.

FIGURE 4. Concrete test block.

sand, and gravel at ratios of 461, 175, 512, and 1252 kg/m^3, respectively. The finished block measured 30 cm in length, 20 cm in width, and 20 cm in height.

The experimental data used in the testing system were sampling signals obtained at the defect-free position of the test block and different penetrating hole defect positions at 5 mm, 7 mm, and 9 mm. The distances between holes were 85 mm. The distance between the hole and the transmitting end of the sensor is 120mm, and the distance between the hole and the receiving end of the sensor is 80mm. Each detection signal contained five cycles, with 20,000 sampling points. The detection position of the concrete is shown in Fig. 5 in which white dots show defect test points and blue dots show defect-free detection positions.

A total of 360 samples of detection data were obtained via the experiment using the testing system which is shown

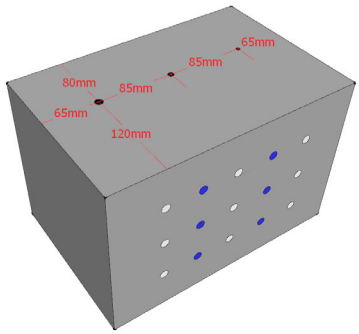

FIGURE 5. Detection location diagram.

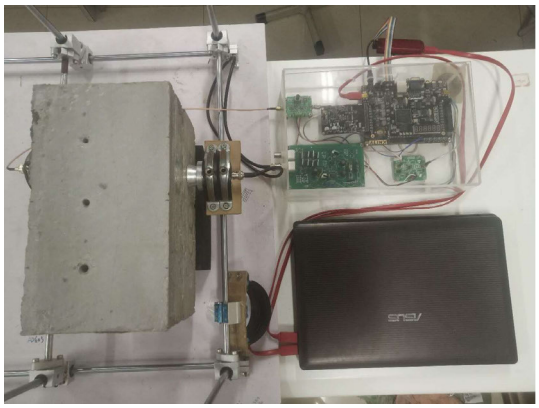

FIGURE 6. Experimental setup test bench.

by Fig. 6. In particular, 180 samples of defect-free detection data and 180 samples of defective detection data have been obtained where the defective data contained 60 samples each for three types of hole defects.

All algorithms described in this paper were run on a computer with 64-bit Windows operation system in which CPU specification is 2.08 GHz, Inter Core i5-8400 with 6 cores and the memory specification is 32GB 2400MHz DDR4, and using the MATLAB® software (R2014a), with the main parameters have been setup and described in the following subsections.

A. STOCHASTIC CONFIGURATION NETWORKS PARAMETERS SETTINGS

These settings include a maximum of 50 hidden layer nodes with training error of 0.01. The activation function used the Log-sigmoid transfer function (logsig) function. The maximum number of random configurations was 100, while the random weight range was {0.5,1,5,10,30,50,100}, the inequality constraint coefficient was {0.9,0.99,0.999,0.9999, 0.99999,0.999999}, and the cumulative step size of the number of hidden layer nodes was 1 [14], [15]. $x = [\bar{z}, \sigma, ku, sk, P]$.

B. K-FOLD CROSS-VALIDATION METHOD PARAMETERS SETTINGS

These were set to as $K = 4, N = 360$. The 360 data samples were randomly divided into four parts, while three of those selected to create a training dataset for the SCNs, and the rest part used as the test dataset. This was performed a total

of four times. We calculated average accuracy based on the accuracy of each test.

C. MATURITY OF THE GENETIC ALGORITHM AND BP NEURAL NETWORK IN OPTIMISATION AND FITTING PERFORMANCE RESEARCH

Compared the calculation results of SCNs with those of genetic algorithm (GA) optimized BP neural network, particularly, we compared and analyzed some advantages and disadvantages of two algorithms in the context of the concrete defect identification in this study. Inclusively, we obtained the optimal number of hidden layer nodes, optimal initial weights and biases. The number of nodes in the hidden layer of the BP neural network involved binary coding, while the corresponding weights and biases involved real coding [27].

D. GENETIC ALGORITHM PARAMETERS SETTINGS

Maximum genetic generation was 100, such that, the genetic algorithm stops after iterating 100 generations, the population size was 30, the length of the binary code was 5, the cross probability was 0.7, and the mutation probability was 0.05.

E. BP NEURAL NETWORK ALGORITHM PARAMETERS SETTINGS

There were five input nodes and two output nodes. Furthermore, there were 13 hidden layer nodes after GA optimization based on the test data. The training stop condition was reached at a training error of 0.01 or 1,000 training times, with a learning rate of 0.05. In the same way, the 4-fold cross-validation was used for the training and testing procedures. In this study, the hyperbolic tangent sigmoid transfer function (tansig) was used for the hidden layer function, while the logsig was used for the output layer.

IV. RUNNING AND ANALYSING THE PROPOSED ALGORITHM

Four typical waveform samples were randomly selected from the original detection signals obtained in the experiment. Fig. 7 shows the last cycle of each signal. It has been shown that the signals are different during the propagation in specific concrete test block.

In particular, the changes of the waveforms shown in Fig. 7 are reflected in both amplitude and spectrum. Therefore, differences between signals can be distinguished in statistics sense based on the signal data in both the frequency and time domains.

Wavelet packet transform was used to decompose the four types of detection waveforms into three layers. Then we obtained eight different frequency band components, which have been illustrated by Figs. 8-11.

As shown in the above figures, the detection signal is decomposed via three-layer wavelet packet, its main frequency band is located at the first node. In other words, the first node of the third layer contains most of the valid information. In contrast, there is more noise arranged in high-frequency components, and less useful information in amplitude and frequency for analyzing detection signals.

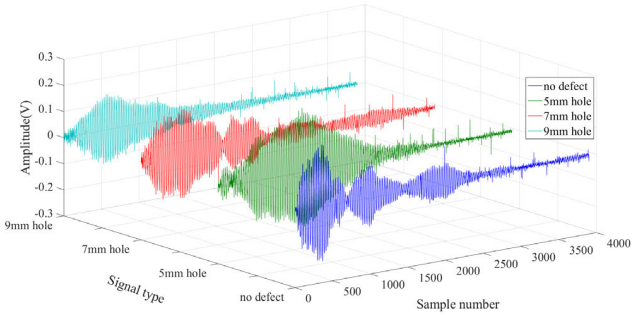

FIGURE 7. Four types of detection waveforms.

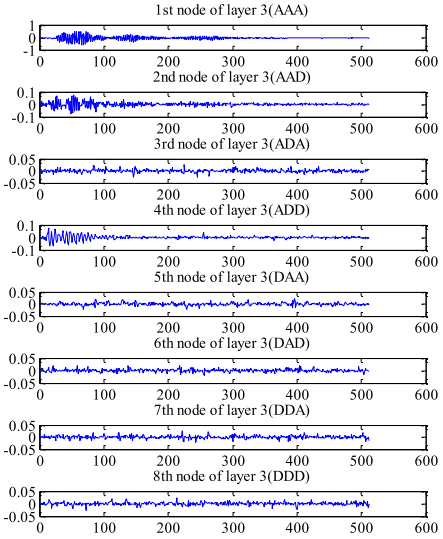

FIGURE 8. Decomposition of signals with no defect.

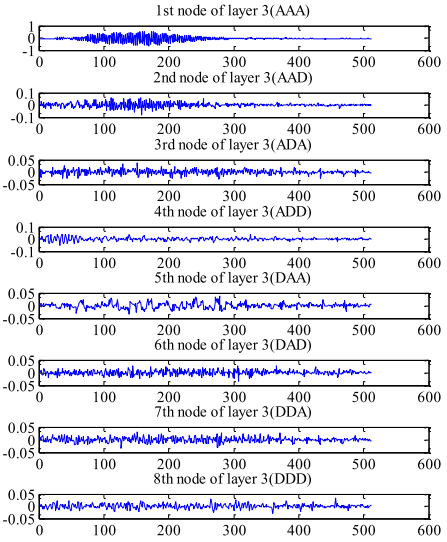

FIGURE 9. Decomposition of signals at 5 mm hole.

Then, the above four types of detection signals are reconstructed according to the wavelet packet coefficients of the first node of the third layer. Therefore, we could analyze extracted feature values and the composition from the reconstructed waveforms. As shown in Fig. 12, the frequency

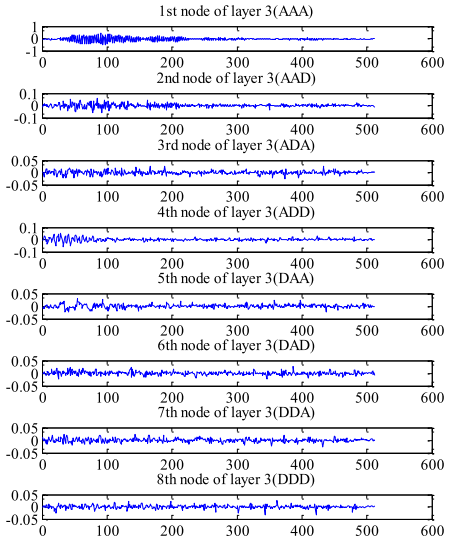

FIGURE 10. Decomposition of signals at 7 mm hole.

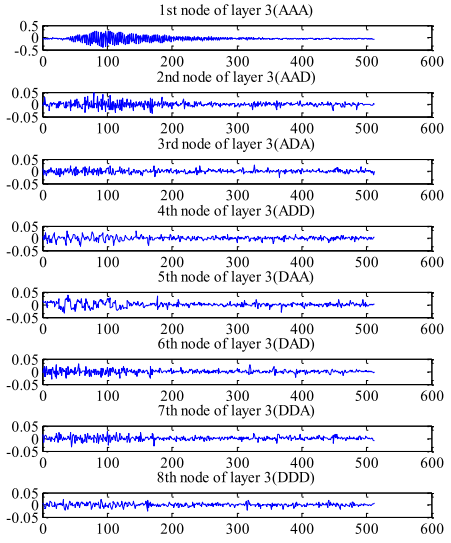

FIGURE 11. Decomposition of signals at 9 mm hole.

of amplitude for the reconstructed waveform is counted to obtain a frequency histogram. The ordinates represent the numbers of discrete points within the signal amplitude ranges.

In addition, the abscissas indicate signal amplitudes, while the ordinates indicate the count values of the discrete points of the signals in the same amplitude ranges. The red curves in Fig. 12 indicate approximate normal distribution curves for the signals. The figure also shows that the non-defective and defective ultrasonic detection signals all approximately obey normal distributions (a mean value of 0). Regarding the standard deviation of the normal distribution, the signal at the5 mm hole was significantly different from the other three types of detection signals. The standard deviations of the non-defective signal and the signal at 7 mm hole were the closest, with the data distributions of the two signals being the most similar. The amplitude ranges of the three types of hole detection signals gradually decreased. It is clearly visible

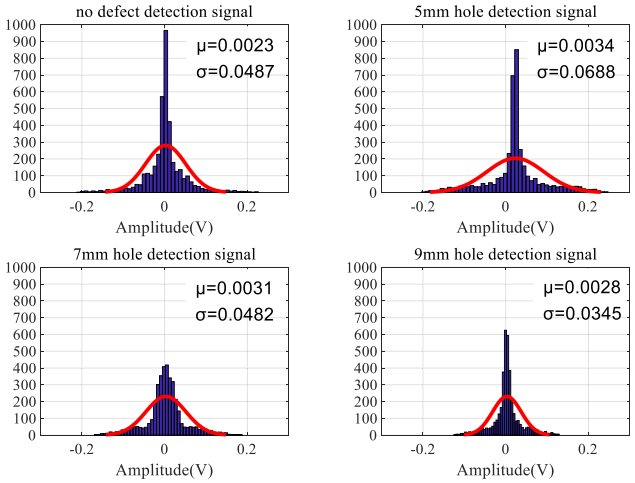

FIGURE 12. Frequency histograms of reconstructed signals amplitude.

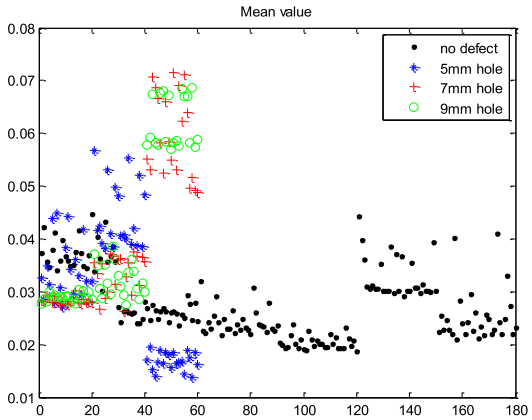

FIGURE 13. Mean values.

in graphic results that the four different detection signals had similarities and differences.

Following the wavelet packet decomposition and reconstruction of the 360 detection signal samples, 5 features were extracted from each reconstructed signal, including mean value, standard deviation, kurtosis coefficient, skewness coefficient, and energy ratio (see Figs. 13-17). As shown by the figures, the abscissas are the numbering of detection samples, while the ordinates are the feature values.

Figs. 13-17 show that different types of detection signals have aliasing in the same feature. Either the non-defective or defective detection signals have no laws that can be separated linearly on the 5 extracted features. It can be noted that the distributions of detection data in different features are of a certain regularity (e.g. the feature values of 5 mm and 9 mm hole-detection data). Since the same detection location was repeatedly tested during the detection process, the detection data will have evident similarities. In addition, the partial data distribution is concentrated (e.g. the kurtosis coefficient of some 9 mm defect detection data, as shown in Fig. 15). However, other data features reflect the reduced aggregation.

In addition, for deeply analyzing the distribution characteristics of extracted features, the box-plot is used for

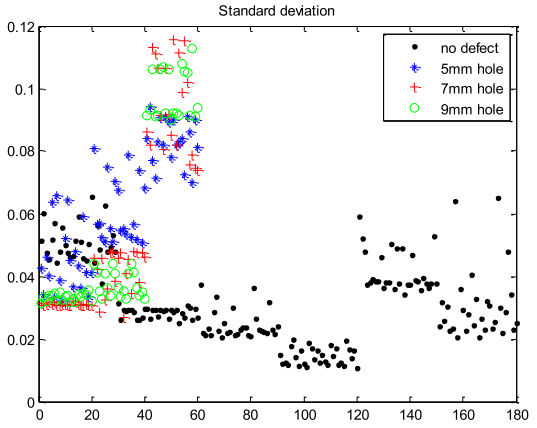

FIGURE 14. Standard deviation values.

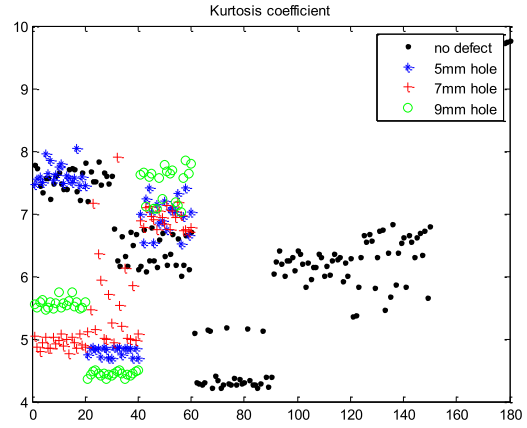

FIGURE 15. Kurtosis coefficients.

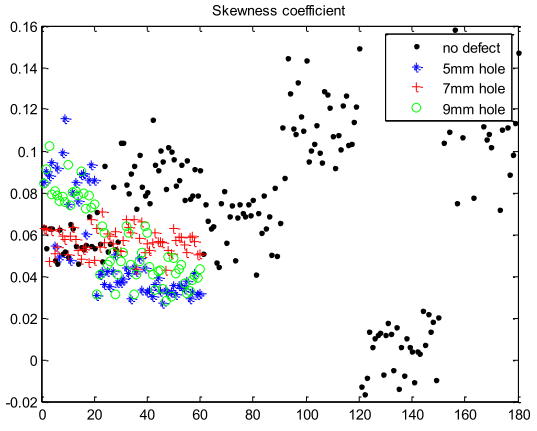

FIGURE 16. Skewness coefficient values.

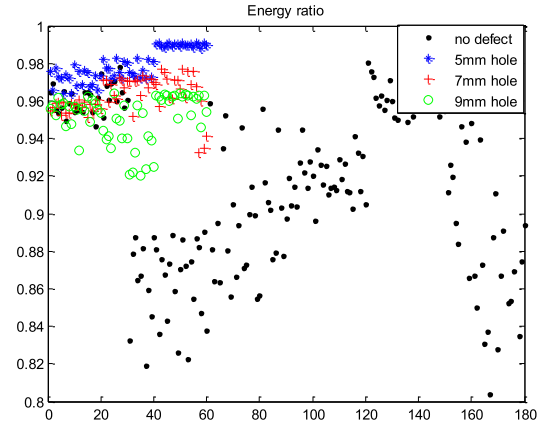

FIGURE 17. Energy ratio values.

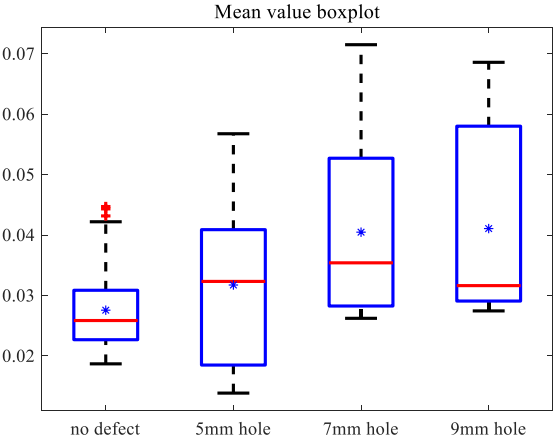

FIGURE 18. Mean values boxplot.

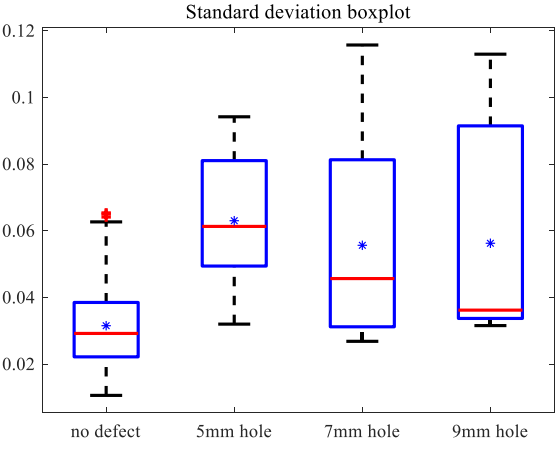

FIGURE 19. Standard deviation values boxplot.

graphical display. As shown in Figs. 18-22, the upper edges of the blue rectangles indicate upper quartile Q3, here, the value is the 75% position of the data in ascending order. The lower edge is referred to as lower quartile Q1 (25% position of the data), the difference between Q3 and Q1 is called the interquartile range IQR. Further, $*$ indicates mean value, while red horizontal lines indicate medians. The upper and lower black short horizontal lines represent the upper and lower edges, respectively, where the value of the upper edge is Q3+1.5IQR, and the value of the lower edge is Q1-1.5IQR (+ is an abnormal value).

In the above boxplots, three types of hole defect signals show relatively similar distributions in terms of the feature values. Meanwhile, there is a certain difference between the distribution of the feature data without defects. The four types of detection data overlap in the extracted feature distribution intervals. As shown in Figs. 18 and 19, the fundamental

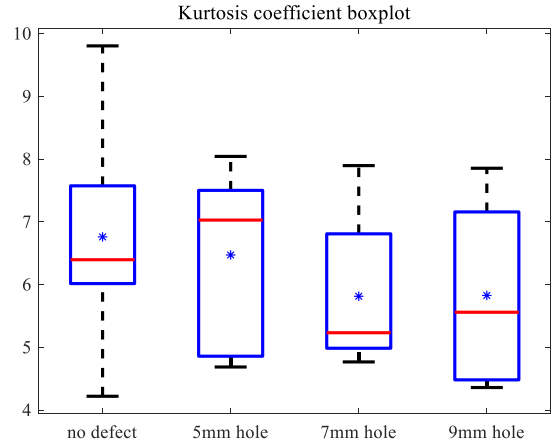

FIGURE 20. Kurtosis coefficient values boxplot.

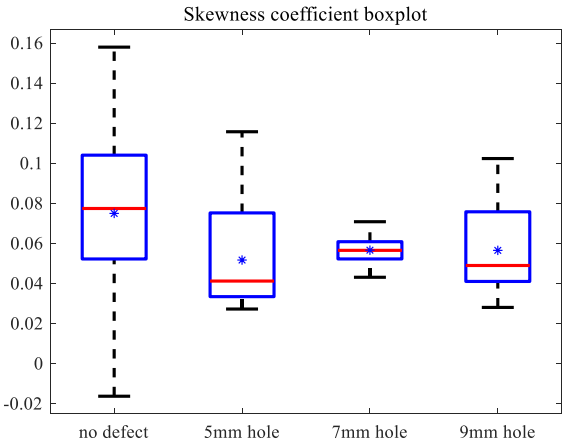

FIGURE 21. Skewness coefficient values boxplot.

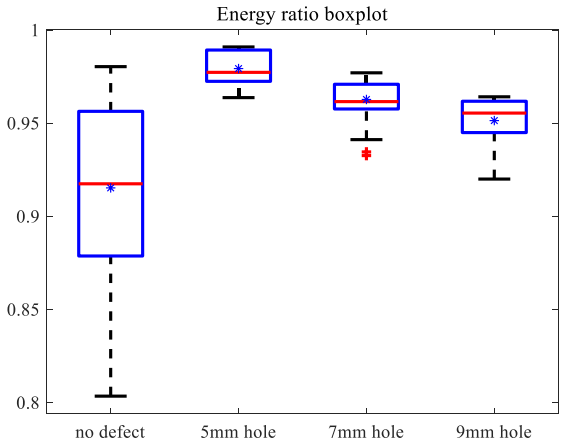

FIGURE 22. Energy ratio values boxplot.

wave data of the non-defective structure are more concentrated in the mean values and standard deviations. However, the distributions in the other three features are more scattered, as shown in Figs. 20-22. For defective fundamental wave data, the distributions of the skewness coefficients and energy ratios are concentrated, while the distributions of the remaining three features are comparatively scattered. In this regard, the differences of distributions for the kurtosis coefficients are more evident. On the other hand, outliers may exist in

TABLE 1. Training dataset recognition results for the two models.

Model	No.	Classes	Result		Accuracy	Average accuracy
			True	False		
GA-BP	1	No defect	131	4	97.41%	97.04%
		Defect	132	3		
	2	No defect	132	3	97.78%	
		Defect	132	3		
	3	No defect	130	5	97.41%	
		Defect	133	2		
	4	No defect	127	8	95.56%	
		Defect	131	4		
SCNs	1	No defect	131	4	98.15%	98.06%
		Defect	134	1		
	2	No defect	133	2	98.89%	
		Defect	134	1		
	3	No defect	130	5	97.78%	
		Defect	134	1		
	4	No defect	130	5	97.41%	
		Defect	133	2		

TABLE 2. Test dataset recognition results for the two models.

Model	No.	Classes	Result		Accuracy	Average accuracy
			True	False		
GA-BP	1	No defect	42	3	93.33%	92.50%
		Defect	42	3		
	2	No defect	41	4	92.22%	
		Defect	42	3		
	3	No defect	41	4	91.11%	
		Defect	41	4		
	4	No defect	42	3	93.33%	
		Defect	42	3		
SCNs	1	No defect	43	2	96.67%	95.34%
		Defect	44	1		
	2	No defect	42	3	95.67%	
		Defect	44	1		
	3	No defect	40	5	93.33%	
		Defect	44	1		
	4	No defect	43	2	96.67%	
		Defect	43	2		

gross error data. If these outliers are not eliminated, it will be an important factor that affects model identification accuracy. Based on the results shown in the above figures, any features extracted from the detection data are not linearly separable. At the same time, the feature vectors formed by those features can be used to classify and identify the signal data of concrete defect structures.

The 4-fold cross-validation method was used when training and testing the SCNs. The feature dataset was randomly divided into four parts where three of them were selected in turn as training datasets, while one was used as the test dataset. A comparison was given using the BP neural network which was optimized by GA (i.e., using the same training and test datasets). The testing results have been shown in Tables 1 and 2 as well as in Fig. 23. Basically, the tables show the detailed recognition results via 4-fold cross-validation of 270 training data and 90 test data. The 90 test data are extracted equally out of the non-defective and defective signals.

As shown in the tables above, both models had recognition accuracy rates greater than 90% which implies the effective identification of defect signals produced by holes

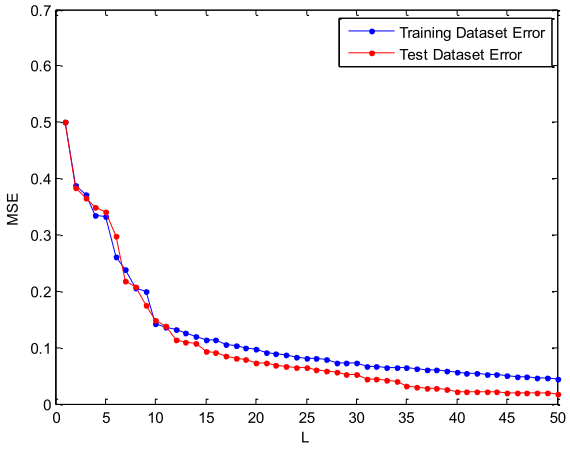

FIGURE 23. SCNs training process error curves.

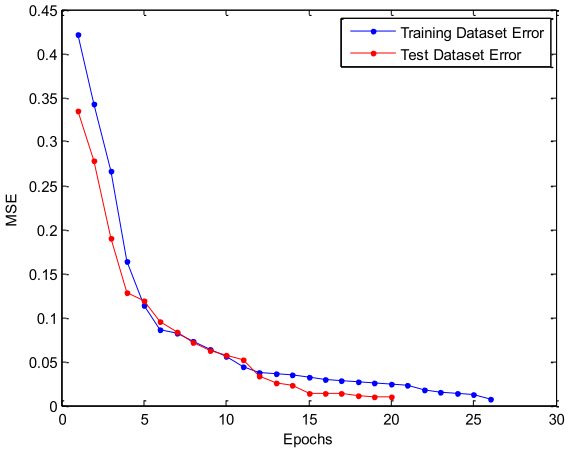

FIGURE 24. GA-BP training process error curves.

in concrete. It is feasible to choose 5 types of statistics as features. Particularly, the recognition accuracies of the SCNs algorithm shown in Table 1 for the training dataset were higher than GA-BP algorithm in general. From the recognition results shown in Table 2, accuracies and average recognitions of SCNs were also higher than those of the GA- optimized BP neural network in all four recognition tests. This proves that SCNs model has better generalization and fitting abilities than GA-BP based on the experimental data.

In addition, the average training time of SCNs was 0.7471s, while the average test time was 0.0058s. On the other hand, the average optimization time of the GA-BP neural network was 658.98s, while the average training time was 0.1427s, and the average test time was 0.0060s. This shows that the GA-BP takes less time to train than the SCNs (i.e. a faster training speed), but the GA process takes more time to optimize the BP neural network. Both SCNs and BP were three-layer network structures. SCNs had more hidden layer nodes than BP, and SCNs needed more training time. After training, the time difference between the two models in testing was very small.

Fig. 23 shows the mean square error curves in both the training dataset and test dataset during the iterative calculation process of SCNs, while Fig. 24 shows the mean square error curves in the same datasets during the iterative calculation process of the GA-BP.

As shown by the error convergence curves of the iterative calculation in Figs. 23-24, the computational time costs of the two algorithms were equivalent, although the abscissas were different. The calculation convergence speeds of the two algorithms were similar only if ignoring the GA-BP optimization time. Each iteration, SCNs added a hidden layer node, an epoch was performed. GA-BP and SCNs began to converge approximately at the 15th epoch. The two algorithms required the same epochs for convergence, but SCNs took more time to perform each epoch than GABP. SCNs changed the model structure by accumulating the number of hidden nodes and evaluated the output weight of the newly added hidden nodes which slowed down the calculation speed of SCNs. Therefore, SCNs had a slightly slower convergence speed than GA-BP while its recognition accuracy was higher. Overall, the proposed SCNs model would lead to better performance for recognition of these concrete defect signals with respect to the computational scale of three-layer neural network.

Concrete is a complex, multiphase, non-uniform medium. For that reason, using ultrasonic methods for concrete detection problems will be complex and diverse due to the complex and uncertain acoustic phenomena, etc. which is the main factor affecting the accuracy of model identification. Based on the experiment, changes of the hardware system outputs resulted in different ultrasonic signal detection data. Moreover, the data contained features with uncertain differences which affected recognition accuracy. In the process of establishing the SCNs recognition model, irrational parameter settings in the network structure may also lead to overfitting, which causes substantial decreases in SCNs recognition accuracy during testing.

V. CONCLUSION AND FUTURE WORKS

This study developed and assessed a method for accurately and reliably realizing the use of ultrasonic detection signals for the purpose of identifying defects in concrete. In particular, the method uses wavelet packet transform to extract the main frequency node of the detection signal which leads to five types of statistics as feature vectors (i.e. mean values, standard deviations, kurtosis coefficients, skewness coefficients, and energy ratios). Then we use the stochastic configuration networks embedded with cross-validation method to identify such defects. We applied the method to experimental data obtained from a C30 class concrete block with penetrating holes. By analyzing the features of the reconstructed signals in different detection positions and assessing statistical relationships between the five aforemen-tioned features, we notice the complexity of the detection signal recognition. Then, we compared the calculation results and algorithmic performances between the presented method and the existing GA-BP algorithm. It has been shown that the SCNs resulted in higher generalization abilities, better

fitting capabilities, and higher recognition accuracy than the GA-BP.

In summary, the experimental results showed the effectiveness of the presented method for identifying concrete hole defects. Based on the excellent performance of the presented algorithm in terms of hole defect signal recognition, future studies should be conducted to identify its ability to detect other defect types, such as cracks and foreign matter inclusions, which are also common defect types in concrete detection. Moreover, the algorithm will also be further improved from the view of non-Gaussian distribution [28] and entropy-based estimation [29], [30] in order to release the Gaussian assumption in Fig. 12.

ACKNOWLEDGMENT

The authors would like to thank two units for their help in designing the hardware system and the actual parameters testing of the ultrasonic probe, Hangzhou Ruidian Meter Company Ltd., and the Shanghai Ultra Precision Motion Control and Detection Engineering Research Center.

REFERENCES

[1] D. A. Clayton and C. M. Smith, "Comparative testing of nondestructive examination techniques for concrete structures," *Proc. SPIE Nondestruct. Characterization Composite Mater., Aerosp. Eng., Civil Infrastruct., Homeland Secur.*, vol. 9063, Mar. 2014, Art. no. 90631G.

[2] M. S. M. Naqiuddin, M. S. Leong, L. M. Hee, and M. A. M. Azrieasrie, "Ultrasonic signal processing techniques for pipeline: A review," *MATEC Web Conf.*, vol. 255, p. 6006, Dec. 2019.

[3] F. Mielentz, V. Feller, M. Krause, R. Orglmeister, and K. Mayer, "Sound field modelling of ultrasonic shear wave probes-modelling of probe arrays with the elastodynamic finite integration technique and point source synthesis," *Mater. Test.*, vol. 55, nos. 11–12, pp. 856–864, 2013.

[4] F. Luo, H. Huang, Y. Duan, J. Liu, and Y. Liao, "Local geometric structure feature for dimensionality reduction of hyperspectral imagery," *Remote Sens.*, vol. 9, no. 8, p. 790, Aug. 2017.

[5] G. Shi, H. Huang, and L. Wang, "Unsupervised dimensionality reduction for hyperspectral imagery via local geometric structure feature learning," *IEEE Geosci. Remote Sens. Lett.*, vol. 17, no. 8, pp. 1425–1429, Aug. 2020.

[6] A. Mostavi, N. Kamali, N. Tehrani, S.-W. Chi, D. Ozevin, and J. E. Indacochea, "Wavelet based harmonics decomposition of ultrasonic signal in assessment of plastic strain in aluminum," *Measurement*, vol. 106, pp. 66–78, Aug. 2017.

[7] S. A. Atashipour, H. R. Mirdamadi, M. H. Hemasian-Etefagh, R. Amirfattahi, and S. Ziaei-Rad, "An effective damage identification approach in thick steel beams based on guided ultrasonic waves for structural health monitoring applications," *J. Intell. Mater. Syst. Struct.*, vol. 24, no. 5, pp. 584–597, Mar. 2013.

[8] Y. Guo, Z. Xiao, L. Geng, J. Wu, F. Zhang, Y. Liu, and W. Wang, "Fully convolutional neural network with GRU for 3D braided composite material flaw detection," *IEEE Access*, vol. 7, pp. 151180–151188, 2019.

[9] S. Saechai, W. Kongprawechnon, and R. Sahamitmongkol, "Test system for defect detection in construction materials with ultrasonic waves by support vector machine and neural network," in *Proc. 6th Int. Conf. Soft Comput. Intell. Syst.*, Nov. 2012, pp. 1034–1039.

[10] A. Drozdov, I. Pomortsev, K. Tyutyukin, and Y. Baloshin, "Comparison of wavelet transform and Foursier transform applied to analysis of nonstationary processes," *Nanosyst. Phys. Chem. Math.*, vol. 5, no. 3, pp. 363–373, 2014.

[11] H.-P. Huang, S.-Y. Wei, H.-H. Chao, C. F. Hsu, L. Hsu, and S. Chi, "An investigation study on mode mixing separation in empirical mode decomposition," *IEEE Access*, vol. 7, pp. 100684–100691, 2019.

[12] N. Munir, H.-J. Kim, J. Park, S.-J. Song, and S.-S. Kang, "Convolutional neural network for ultrasonic weldment flaw classification in noisy conditions," *Ultrasonics*, vol. 94, pp. 74–81, Apr. 2019.

[13] N. Nishida, M. Yamakawa, T. Shiina, and M. Kudo, "Current status and perspectives for computer-aided ultrasonic diagnosis of liver lesions using deep learning technology," *Hepatol. Int.*, vol. 13, pp. 416–421, Feb. 2019.

[14] D. Wang and M. Li, "Stochastic configuration networks: Fundamentals and algorithms," *IEEE Trans. Cybern.*, vol. 47, no. 10, pp. 3466–3479, Oct. 2017.

[15] D. Wang and M. Li, "Robust stochastic configuration networks with kernel density estimation for uncertain data regression," *Inf. Sci.*, vols. 412–413, pp. 210–222, Oct. 2017.

[16] H. Qu, T. Feng, Y. Zhang, and Y. Wang, "Ensemble learning with stochastic configuration network for noisy optical fiber vibration signal recognition," *Sensors*, vol. 19, no. 15, p. 3293, Jul. 2019.

[17] A. Gupta and J. C. Duke, "Identifying the arrival of extensional and flexural wave modes using wavelet decomposition of ultrasonic signals," *Ultrasonics*, vol. 82, pp. 261–271, Jan. 2018.

[18] S. Hamsa, I. Shahin, Y. Iraqi, and N. Werghi, "Emotion recognition from speech using wavelet packet transform cochlear filter bank and random forest classifier," *IEEE Access*, vol. 8, pp. 96994–97006, 2020.

[19] A. Cardinali and G. P. Nason, "Locally stationary wavelet packet processes: Basis selection and model fitting," *J. Time Ser. Anal.*, vol. 38, no. 2, pp. 151–174, Mar. 2017.

[20] K. Manjula, K. Vijayarekha, and B. Venkatraman, "Quality enhancement of ultrasonic TOFD signals from carbon steel weld pad with notches," *Ultrasonics*, vol. 84, pp. 264–271, 2018.

[21] H. Guo, F. Qin, B. Zheng, and Y. Wang, "Neural network identification of defect statistics characteristics in laser ultrasonic," *Appl. Laser*, vol. 37, no. 6, pp. 888–892, 2017.

[22] X. Wang, S. Guan, L. Hua, B. Wang, and X. He, "Classification of spot-welded joint strength using ultrasonic signal time-frequency features and PSO-SVM method," *Ultrasonics*, vol. 91, pp. 161–169, Jan. 2019.

[23] P. Yan, M. K. Liu, and H. Ma, "Design of ultrasonic testing system and analysis of echo signal characteristics," *Electron. Meas. Technol.*, vol. 42, no. 2, pp. 123–129, 2019.

[24] W. Wang, K. Li, K. Cai, and D. He, "Analysis of ammonia nitrogen concentration using stochastic configuration networks," in *Proc. Chin. Autom. Congr. (CAC)*, Nov. 2018, pp. 903–906.

[25] J. Yang, C.-Q. Gao, and X.-F. Liu, "Affect of different simulation mode on ultrasonic testing signal," *Nondestruct. Test.*, vol. 32, no. 1, pp. 36–38, 2010.

[26] N. Kamal, A. Lahgere, and J. Singh, "Evaluation of radiation resiliency on emerging junctionless/dopingless devices and circuits," *IEEE Trans. Device Mater. Rel.*, vol. 19, no. 4, pp. 728–732, Dec. 2019.

[27] J. Peng, W. Lv, H. Xing, and X. Wu, "Temperature compensation for humidity sensor based on improved GA-BP neural network," *Chin. J. Sci. Instrum.*, vol. 34, no. 1, pp. 153–160, 2013.

[28] M. Ren, Q. Zhang, and J. Zhang, "An introductory survey of probability density function control," *Syst. Sci. Control Eng.*, vol. 7, no. 1, pp. 158–170, Jan. 2019.

[29] X. Yin, Q. Zhang, H. Wang, and Z. Ding, "RBFNN-based minimum entropy filtering for a class of stochastic nonlinear systems," *IEEE Trans. Autom. Control*, vol. 65, no. 1, pp. 376–381, Jan. 2020.

[30] Q. Zhang and U. Department of Computer Science University of BradfordBradfordBD7 1DP, "Performance enhanced Kalman filter design for non-Gaussian stochastic systems with data-based minimum entropy optimisation," *AIMS Electron. Electr. Eng.*, vol. 3, no. 4, pp. 382–396, 2019.

JINHUI ZHAO (Member, IEEE) received the B.Sc. degree from Northeastern University, in 1997, the M.Sc. degree from Liaoning Technical University, in 2006, and the Ph.D. degree from Zhejiang University, in 2010. She is currently an Associate Professor with the Zhejiang University of Water Resources and Electric Power. Her main research interests include computational intelligence, data analysis and uncertainty quantification, ultrasonic testing, signal processing, and pattern recognition.

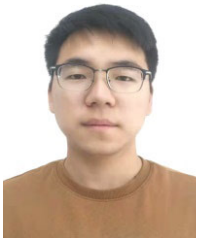

TIANYU HU was born in Suzhou, China, in 1996. He received the bachelor's degree from West Anhui University, in 2017. He is currently pursuing the master's degree with China Jiliang University. His main research interests include signal processing and pattern recognition.

RUIFANG ZHENG received the bachelor's and master's degrees from China Jiliang University in 2016 and 2020, respectively. His research interests include signal processing, modeling and simulation, and hardware circuit design.

PENGHUI BA received the bachelor's degree from the Yangtze River College, East China Institute of Technology, in 2019. He is currently pursuing the master's degree with China Jiliang University. His main research interests include instrumentation, signal processing, and testing.

CONGLI MEI received the B.Sc. and M.Sc. degrees in automatic control from Jiangsu University, China, in 2001 and 2004, respectively, and the Ph.D. degree in automatic control from Zhejiang University, China, in 2007. He is currently a Professor with the Zhejiang University of Water Resources and Electric Power, China. His research interests include intelligent control, data analysis, design, and control of PMSMs.

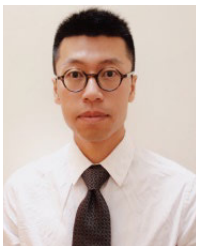

QICHUN ZHANG (Senior Member, IEEE) received the B.Eng. degree in automation and the M.Sc. degree in control theory and control engineering from Northeastern University, China, in 2008 and 2010, respectively, and the Ph.D. degree in electrical and electronic engineering from the University of Manchester, U.K., in 2016. He was a Senior Lecturer in dynamics and control with De Montfort University, a Senior Research Officer in neural engineering with the University of Essex, and an Academic Visitor with the Control Systems Centre, University of Manchester. He is currently a Lecturer in computer science with the University of Bradford, U.K. His research interests include stochastic dynamic systems, probabilistic coupling analysis, decoupling control, performance optimization, brain–computer interface, and computational modeling for peripheral nervous systems. He serves more than 20 international journals as an Active Reviewer. He is an Associate Editor of IEEE Access and *Journal of Intelligent Manufacturing*. He is an Academic Editor of *PLoS ONE* and *PeerJ Computer Science* and an Editorial Board Member of other four journals.